Available online at www.sciencedirect.com
SCIENCE DIRECT
Composites: Part A 36 (2005) 1142–1151
composites Part A: applied science and manufacturing
www.elsevier.com/locate/compositesa

Stress transfer for a SMA fiber pulled out from an elastic matrix and related bridging effect

Xiaoling Wang, Gengkai Hu*

Department of Applied Mechanics, Beijing Institute Technology, No. 7 BaiShiQiao Road, Beijing 100081, China

Received 2 May 2004; revised 10 December 2004; accepted 23 December 2004

Abstract

An analytical model is proposed to examine the stress transfer for a Shape Memory Alloy (SMA) fiber pulled out from an elastic matrix, the transformation characteristic of the SMA fiber and the influence of temperature are considered. The embedded SMA fiber is divided into a full transformation region, a partial transformation region and an intact region. The shear-lag model is utilized to analyze the stress distribution during the pulled-out of the SMA fiber. Compared to an elastic fiber pulled out from an elastic matrix, the transformation induced in the SMA fiber significantly lowers the axial stress, and the lateral contraction due to the transformation increases significantly the radial stress. Temperature has also an important influence on the stress distribution by alternating the transformation characteristic of the SMA material. The obtained results are then applied to analyze the bridging effect due to the SMA fiber, the computed results show that an increase of temperature decreases the stress intensity factor, which is in agreement with experimental observation in the literature. These results are useful for the design of intelligent composite materials.

Keywords: SMA fiber

1. Introduction

Shape Memory Alloys (SMAs) can undergo a reversible phase transformation under a proper thermo-mechanical loading, they are widely used as actuators or sensors in active composite materials. For example in form of fibers, they can be embedded into a matrix material to form SMA composite. This composite, with a careful design, can have the desired properties, such as very low thermal expansion under thermal loading [1]. SMAs are also widely used in vibration control systems [2,3], for more applications, one can refer to the review paper given by Birman [4]. The mechanical response of a composite with SMA fibers has been recently studied by Song et al. [5]. The shape memory alloy (SMA), which is an effective actuator in smart structures, is often embedded in a host material. If a crack is initiated in the matrix, SMA fibers can be used to prevent crack propagation and even to close the generated crack [4], this concept is demonstrated experimentally by Eisaku [6]. One of the key issues is the requirement of good stress transfer between SMA fiber and host material, Jonnalagadda et al. [7] examined experimentally the local stress transfer for a SMA fiber embedded in a matrix material. For a SMA ribbon pulled-out from a host material, Jonnalagadda et al. [8] performed an in situ displacement measurements, they also proposed the corresponding numerical analysis for this pulled-out process, the theoretical results compared favorably with the experimental results. To examine the bridging effect due to SMA fibers, the bridging law, determined by analysis of a SMA fiber pulled out from a host material, is needed, however, an analytical method for this process is not available.

Stress transfer between fiber and matrix is one of fundamental issues for a composite system. Over the past few decades, there were a large amount of publications devoted to better understanding this mechanism. The shear-lag model is widely accepted and utilized to analyze this stress transfer [9,10], the accuracy of this method has been discussed by Nairn [11]. Many refined shear-lag models have been developed since then, to cite a few for example, Hutchinson et al. [12] proposed a systematic analysis for

* Corresponding author. Tel.: +86 106 891 2731; fax: +86 106 891 4780.
E-mail address: hugeng@public.bta.net.cn (G. Hu).

1359-835X/$ - see front matter © 2005 Elsevier Ltd. All rights reserved.
doi:10.1016/j.compositesa.2005.01.001

a transversely isotropic fiber pulled out from an elastic matrix, Hsueh [13] gave also a method, in which the radial dependences of axial stresses in both fiber and matrix were included. Fu et al. [14] advanced a more refined model, which satisfies necessary conditions such as equilibrium equations, boundary condition and continuity condition, fiber's interaction is also taken into account. Most of these works are concerned with stress transfer mechanism for an elastic fiber and an elastic matrix, only few tackle the nonlinear fiber or matrix [15–17]. The objective of this paper is to propose a simple analytical model for a SMA fiber pulled out from an elastic matrix, and to get some basic insights on influence of different parameters, and then the results are utilized to calculate the corresponding bridging law necessary for a subsequent analysis.

The manuscript will be organized as follows: the theoretical analysis of a SMA fiber pulled out from an elastic matrix will be presented in Section 2, in which the transformation characteristic of the SMA material, model assumptions are explained in details; some numerical applications for analyzing the influence of different parameters, such as volume fraction of SMA fibers and temperature, are also provided. In Section 3, the influence of SMA fiber bridging on stress intensity factor will be examined, and followed by a summary in Section 4.

2. Stress transfer for a SMA fiber pulled out from an elastic matrix

2.1. Constitutive relation for a SMA fiber

In this paper, the three-dimensional constitutive equation proposed by Lagoudas et al. [18] will be utilized. During the forward transformation (Austenite–Martensite), the transformation strain can be written as

$$\varepsilon_{ij}^{t} = \Lambda_{ij}\xi \tag{1}$$

where the transformation tensor is given by

$$\Lambda_{ij} = -\frac{3}{2}\frac{\Omega}{E^{f}}\bar{\sigma}^{-1}\sigma'_{ij} \tag{2}$$

and $\bar{\sigma} = (3\sigma'_{ij}\sigma'_{ij}/2)^{1/2}$, the deviatoric stress σ'_{ij} is defined by $\sigma'_{ij} = \sigma_{ij} - \sigma_{kk}\delta_{ij}/3$, Ω/E^{f} is the maximum transformation strain, ξ is the volume fraction of the martensite during the forward transformation, and it is related to stress and temperature by [18]

$$\xi = 1 - \exp[a^{M}(M^{os} - T) + b^{M}\bar{\sigma}], \quad M^{f} \le T \le M^{s} \tag{3}$$

where $a^{M} = \ln(0.01)/(M^{os} - M^{of})$, $b^{M} = a^{M}/C^{M}$ and C^{M} is the influence coefficient of the martensite. M^{os}, M^{of} are the martensite transformation start and finish temperatures in a stress-free state, respectively; M^{s}, M^{f} are those under the stress $\bar{\sigma}$. A sketch of the transformation diagram for a SMA material is illustrated schematically in Fig. 1.

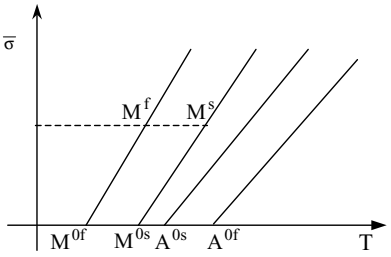

Fig. 1. Transformation diagram of a SMA material.

For an initial austenite state, once transformation from austenite to martensite takes place, the resulted SMA material is in fact a mixture of the martensite and the austenite phases. Its overall properties such as the modulus, Poisson's ratio and thermal expansion coefficient have to be determined by a proper micromechanical approach [19–21], or simply by a mixture law [18]. In this paper, the Young's modulus, Poisson's ratio and thermal expansion coefficients of the martensite and the austenite are taken to be the same. (Note: in NiTi polycrystal, the Young's modulus of austenite is the same order as that of the martensite). The purpose of the above assumption is to simplify the subsequent analysis and to make an analytical solution possible. Furthermore, a linear expansion of Eq. (3) is made for further simplification

$$\xi = 1 - (\exp[\bar{a}^{M}(M^{os} - T)] + \exp[\bar{a}^{M}(M^{os} - T)]\bar{b}^{M}\bar{\sigma}),$$
$$M^{f} \le T \le M^{s} \tag{4}$$

where $\bar{a}^{M}$, $\bar{b}^{M}$ are the constants to better fit Eq. (3).

2.2. Description and assumptions of the model

As shown in Fig. 2, a two concentric cylinder model is employed to elucidate the stress transfer mechanism between a SMA fiber and its host material. A stress σ_a is applied on the SMA fiber, the other end is assumed to be stress free (no end stress). The bottom side of the cylinder is fixed and the outer

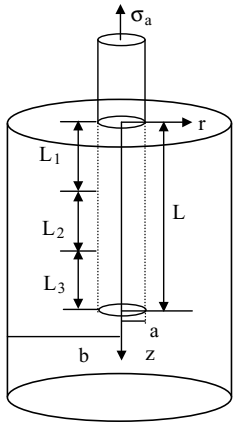

Fig. 2. Sketch of the model.

lateral surface of the cylinder is taken to be stress free. A pressure can be included without any difficulty to simulate residual stress or finite concentration of the SMA fibers. The whole problem is axisymmetric, the radii of the fiber and the outer cylinder are denoted by a and b, respectively.

Due to the applied stress σ_a and the constraint of the matrix, transformation will take place in the SMA fiber. Here for simplification, no debonding is allowed in the analysis. The embedded SMA fiber can be characterized as: a full transformation region of a length L_1, a partial transformation region (L_2) and no transformation region with a length L_3, as shown schematically in Fig. 2. They will be determined in the following analysis.

2.3. Governing equations

Since the problem is axisymmetric, the SMA fiber and the matrix are both isotropic, and their elastic constants and thermal expansion coefficients are assumed to be independent of temperature The total strain in the SMA fiber is the summation of the elastic strain, the transformation strain and the thermal strain induced by temperature variation, so the relations between stress, strain and displacements are given by [22]

$$\varepsilon_r^i = \frac{\partial u_r^i}{\partial r} = \frac{1}{E^i}[\sigma_r^i - \nu^i(\sigma_\theta^i + \sigma_z^i)] + \vartheta^i \varepsilon_r^t + \alpha^i \delta T \tag{5a}$$

$$\varepsilon_\theta^i = \frac{u_r^i}{r} = \frac{1}{E^i}[\sigma_\theta^i - \nu^i(\sigma_r^i + \sigma_z^i)] + \vartheta^i \varepsilon_\theta^t + \alpha^i \delta T \tag{5b}$$

$$\varepsilon_z^i = \frac{\partial u_z^i}{\partial z} = \frac{1}{E^i}[\sigma_z^i - \nu^i(\sigma_\theta^i + \sigma_r^i)] + \vartheta^i \varepsilon_z^t + \alpha^i \delta T \tag{5c}$$

where $i=f, m$, the superscript m denotes the quantity related to the matrix and f to the SMA fiber, respectively. $\vartheta^f=1$, $\vartheta^m=0$, $\delta T=T-T_0$, T_0 is a reference temperature. E, ν and α denote Young's modulus, Poisson's ratio and thermal expansion coefficient, respectively. $\varepsilon_n^t (n=r,\theta,z)$ are the transformation strains presented in the SMA fiber, and zero in the matrix.

The equilibrium equation of an axisymmetric problem is written as [22]:

$$\frac{\partial \sigma_r}{\partial r} + \frac{\partial \tau_{zr}}{\partial z} + \frac{\sigma_r - \sigma_\theta}{r} = 0 \tag{6a}$$

$$\frac{\partial \sigma_z}{\partial z} + \frac{\partial \tau_{rz}}{\partial r} + \frac{\tau_{rz}}{r} = 0 \tag{6b}$$

2.4. Solution of the problem

The solution of Eqs. (5a)–(6b) leads to the following expressions for the stresses in the fiber and in the matrix, respectively:

$$\sigma_{rj}^m = \frac{B_j}{r^2} + C_j, \quad \sigma_{\theta j}^m = -\frac{B_j}{r^2} + C_j \tag{7}$$

$$\sigma_{rj}^f = \sigma_{\theta j}^f = A_j \tag{8}$$

The index $j=1$–3, corresponding to the full transformation region, partial transformation and no transformation regions, respectively. A_j, B_j and C_j are the coefficients to be determined, and they are function of the axial position z.

For perfect bonding, the following boundary and continuity conditions are available

$$\sigma_r^m(r=b)=0, \quad [\sigma_r]_{r=a}=0, \quad [u_r]_{r=a}=0 \tag{9}$$

where $[a]=a^+-a^-$, denoting the jump of the quantity a. In the following, we will determine the stress distributions in these three regions.

(a) Fully transformed region

Since the interface between the fiber and the matrix remains intact, and the transformation is complete, this means from Eqs. (1) and (2) that $\varepsilon_{z1}^t=-\Omega/E^f$, $\varepsilon_{\theta 1}^t=\varepsilon_{r1}^t=-\varepsilon_{z1}^t/2$. With these transformation strains, and the boundary and interfacial continuity conditions, it has:

$$\begin{aligned}
&\frac{B_1}{b^2} + C_1 = 0,\\
&\frac{B_1}{a^2} + C_1 = A_1 \frac{1}{E^f}\left[A_1 - \nu^f\left(A_1 + \sigma_{z1}^f\right)\right] + \varepsilon_{\theta 1}^t\\
&\qquad = \frac{1}{E^m}\left[-\frac{B_1}{a^2} + C_1 - \nu^m\left(\frac{B_1}{a^2} + C_1 + \sigma_{z1}^m\right)\right]\\
&\qquad\quad + (\alpha^m - \alpha^f)\delta T
\end{aligned} \tag{10}$$

(b) Partially transformed region

In this region, the transformation is incomplete, the transformation strain depends on volume fraction of martensite in the SMA fiber, in turn on the stress state and temperature in the fiber. With help of the transformation characteristic of the SMA fiber (Eqs. (1), (2) and (4)), and the stress state in the SMA fiber (Eq. (8)), the transformed strain can be expressed by: $\varepsilon_{\theta 2}^t = D_{t21\theta} + D_{t22\theta}(A_2 - \sigma_{z2}^f)$, and $D_{t21\theta} = (\Omega/2E^f) - (\Omega/2E^f)\exp[a^M(M^{os} - T)]$, $D_{t22\theta} = -(\Omega/2E^f)\bar{b}^M \exp[\bar{a}^M(M^{os} - T)]$.

The boundary condition and the continuity conditions provide the following equations to determine the unknown coefficients:

$$\begin{aligned}
&\frac{B_2}{b^2} + C_2 = 0,\\
&\frac{B_2}{a^2} + C_2 = A_2 \frac{1}{E^f}\left[A_2 - \nu^f\left(A_2 + \sigma_{z2}^f\right)\right] + \varepsilon_{\theta 2}^t\\
&\qquad = \frac{1}{E^m}\left[-\frac{B_2}{a^2} + C_2 - \nu^m\left(\frac{B_2}{a^2} + C_2 + \sigma_{z2}^m\right)\right]\\
&\qquad\quad + (\alpha^m - \alpha^f)\delta T
\end{aligned} \tag{11}$$

(c) No transformation region

Since there is no transformation in this region, the boundary and continuity conditions provide:

$$\begin{aligned}
&\frac{B_3}{b^2} + C_3 = 0,\\
&\frac{B_3}{a^2} + C_3 = A_3\frac{1}{E^{\mathrm{f}}}\left[A_3 - \nu^{\mathrm{f}}\left(A_3 + \sigma^{\mathrm{f}}_{z3}\right)\right]\\
&\qquad = \frac{1}{E^{\mathrm{m}}}\left[-\frac{B_3}{a^2} + C_3 - \nu^{\mathrm{m}}\left(\frac{B_3}{a^2} + C_3 + \sigma^{\mathrm{m}}_{z3}\right)\right]\\
&\qquad + (\alpha^{\mathrm{m}} - \alpha^{\mathrm{f}})\delta T
\end{aligned} \tag{12}$$

In above equations, σ^{m}_{zj}, σ^{f}_{zj} are, respectively, the average stresses in the matrix and in the fiber in a plan perpendicular to z-axis, they depend on the axial position z. The global equilibrium relation gives

$$\sigma^{\mathrm{m}}_{zj}(z) = \gamma(\sigma_a - \sigma^{\mathrm{f}}_{zj}(z)) \tag{13}$$

where γ characterizes the volume ratio between SMA fiber and matrix, defined by $\gamma = a^2/(b^2 - a^2)$. From Eqs. (11)–(13), A_j, B_j and C_j can be expressed as functions of the axial stress in the fiber by:

$$A_j = D_j + G_j\bar{\sigma}^{f}_{zj}(z), \quad B_j = \gamma b^2\alpha A_j, \quad C_j = -\gamma\alpha A_j \tag{14}$$

The coefficients D_j and G_j are, respectively

$$D_1 = [\varepsilon^{\mathrm{t}}_{\theta 1} + (\alpha^{\mathrm{f}} - \alpha^{\mathrm{m}})\delta T + \alpha\gamma\nu^{\mathrm{m}}\bar{\sigma}_a]/(-1 - 2\gamma\alpha - \alpha + \nu^{\mathrm{f}} - \alpha\nu^{\mathrm{m}})$$

$$D_2 = [D_{t21\theta} + (\alpha^{\mathrm{f}} - \alpha^{\mathrm{m}})\delta T + \alpha\gamma\nu^{\mathrm{m}}\bar{\sigma}_a]/(1 - 2\gamma\alpha - \alpha + \nu^{\mathrm{f}} - \alpha\nu^{\mathrm{m}} + D_{t22\theta}E^{\mathrm{f}})$$

$$D_3 = [(\alpha^{\mathrm{f}} - \alpha^{\mathrm{m}})\delta T + \alpha\gamma\nu^{\mathrm{m}}\bar{\sigma}_a]/(-1 - 2\gamma\alpha - \alpha + \nu^{\mathrm{f}} - \alpha\nu^{\mathrm{m}})$$

$$G_1 = G_3 = (-\nu^{\mathrm{f}} - \alpha\gamma\nu^{\mathrm{m}})/(-1 - 2\gamma\alpha - \alpha + \nu^{\mathrm{f}} - \alpha\nu^{\mathrm{m}})$$

$$G_2 = (-\nu^{\mathrm{f}} - \alpha\gamma\nu^{\mathrm{m}} + D_{t22\theta}E^{\mathrm{f}})/(1 - 2\gamma\alpha - \alpha + \nu^{\mathrm{f}} - \alpha\nu^{\mathrm{m}} + D_{t22\theta}E^{\mathrm{f}})$$

where $\bar{\sigma}^{\mathrm{f}}_{zj} = \sigma^{\mathrm{f}}_{zj}/E^{\mathrm{f}}$, $\bar{\sigma}_a = \sigma_a/E^{\mathrm{f}}$ and $\alpha = E^{\mathrm{f}}/E^{\mathrm{m}}$.

To determine the axial stress in the SMA fiber, here we will recall the shear-lag model. Take a slice of the SMA fiber, $\tau_j(z)$ is the interfacial shear stress, the equilibrium of this slice leads to:

$$\frac{\mathrm{d}\sigma^{\mathrm{f}}_{zj}(z)}{\mathrm{d}z} = -\frac{2}{a}\tau_j(z) \tag{15}$$

The shear stress in the matrix $\tau^{\mathrm{m}}(r,z)$ has a Lame's form [14], with help of the boundary conditions $\tau^{\mathrm{m}}_j(a,z) = -\tau_j(z)$ and $\tau^{\mathrm{m}}_j(b,z) = 0$, it can be determined as [14]:

$$\tau^{\mathrm{m}}_j(r,z) = -\frac{(b^2 - r^2)/r}{(b^2 - a^2)/a}\tau_j(z) \tag{16}$$

With the constitutive relation of the matrix, and we assume that the displacement components in the radial and circumferential directions can be neglected compared to the axial displacement component [14], then a simplified expression for the shear stress in the matrix can be written as:

$$\tau^{\mathrm{m}}_j(r,z) = G^{\mathrm{m}}\,\mathrm{d}u^{\mathrm{m}}_j(r,z)/\mathrm{d}r \tag{17}$$

G^{m} is the shear modulus of the matrix, and integrating Eq. (17), we get:

$$u^{\mathrm{m}}_j(r,z) - u^{\mathrm{m}}_j(a,z) = -\frac{b^2\ln(r/a) - (1/2)(r^2 - a^2)}{G^{\mathrm{m}}(b^2 - a^2)/a}\tau_j(z) \tag{18}$$

Averaging the both sides of Eq. (17) over the matrix domain, and differentiating the obtained equation with respect to the coordinate z, together with $u^{\mathrm{m}}_j(a,z) = u^{\mathrm{f}}_j(z)$ and constitutive relations for the matrix and the SMA fiber, we have:

$$\begin{aligned}
&\frac{1}{E^{\mathrm{m}}}[\sigma^{\mathrm{m}}_{zj} - \nu^{\mathrm{m}}(\sigma^{\mathrm{m}}_{\theta j} + \sigma^{\mathrm{m}}_{rj})] + \alpha^{\mathrm{m}}\delta T\\
&\quad = \frac{1}{E^{\mathrm{f}}}[\sigma^{\mathrm{f}}_{zj} - \nu^{\mathrm{f}}(\sigma^{\mathrm{f}}_{\theta j} + \sigma^{\mathrm{f}}_{rj})] + \varepsilon^{\mathrm{t}}_{zj} + \alpha^{\mathrm{f}}\delta T - \frac{g}{G^{\mathrm{m}}}\frac{\mathrm{d}\tau_j(z)}{\mathrm{d}z}
\end{aligned} \tag{19}$$

where $\varepsilon^{\mathrm{t}}_{z1} = -\Omega/E^{\mathrm{f}}$, $\varepsilon^{\mathrm{t}}_{z2} = D_{t21z} + D_{t22z}(A_2 - \sigma^{\mathrm{f}}_{z2})$, $\varepsilon^{\mathrm{t}}_{z3} = 0$ and

$$D_{t21z} = -\frac{\Omega}{E^{\mathrm{f}}} + \frac{\Omega}{E^{\mathrm{f}}}\exp[\bar{a}^{\mathrm{M}}(M^{\mathrm{os}} - T)],$$

$$D_{t22z} = \frac{\Omega}{E^{\mathrm{f}}}\bar{b}^{\mathrm{M}}\exp[\bar{a}^{\mathrm{M}}(M^{\mathrm{os}} - T)]$$

$$g = \frac{1}{2}a\left[(1+\gamma)^2\ln\left(\frac{1+\gamma}{\gamma}\right) - \left(\frac{3}{2} + \gamma\right)\right]$$

With help of Eqs. (13)–(15) and (19), the governing differential equation for determining the axial stress $\bar{\sigma}^{\mathrm{f}}_{zj}$ can be written in a compact form for the three regions as

$$\frac{\mathrm{d}^2\bar{\sigma}^{\mathrm{f}}_{zj}(\bar{z})}{\mathrm{d}\bar{z}^2} - g_{j1}\bar{\sigma}^{\mathrm{f}}_{zj}(\bar{z}) + g_{j2} = 0 \tag{20}$$

where $\bar{z} = z/a$, and the coefficients in Eq. (20) are listed in Appendix.

The boundary and continuity conditions will provide the necessary equations to determine the integrated constants

$$\begin{aligned}
&\bar{\sigma}^{\mathrm{f}}_z(0) = \bar{\sigma}_a, \quad \bar{\sigma}^{\mathrm{f}}_z(l) = 0 \quad \bar{\sigma}^{\mathrm{f}}_{z1}(l_1) = \bar{\sigma}^{\mathrm{f}}_{z2}(l_1),\\
&u^{\mathrm{f}}_{z1}(l_1) = u^{\mathrm{f}}_{z2}(l_1) \quad \bar{\sigma}^{\mathrm{f}}_{z2}(l_1 + l_2) = \bar{\sigma}^{\mathrm{f}}_{z3}(l_1 + l_2),\\
&u^{\mathrm{f}}_{z2}(l_1 + l_2) = u^{\mathrm{f}}_{z3}(l_1 + l_2)
\end{aligned} \tag{21}$$

where $l_i = L_i/a$, $l = L/a$.

Since, the phase transformation in the SMA fiber is also continuous, Eq. (4) further provides the following

conditions to determine the transformed and partially transformed region size:

$$\xi(l_1) = 1 - (\exp[\bar{a}^{\mathrm{M}}(M^{\mathrm{os}} - T)] + \exp[\bar{a}^{\mathrm{M}}(M^{\mathrm{os}} - T)]\bar{b}^{\mathrm{M}}\bar{\sigma}) = 1 \tag{22a}$$

$$\xi(l_1 + l_2) = 1 - (\exp[\bar{a}^{\mathrm{M}}(M^{\mathrm{os}} - T)] + \exp[\bar{a}^{\mathrm{M}}(M^{\mathrm{os}} - T)]\bar{b}^{\mathrm{M}}\bar{\sigma}) = 0 \tag{22b}$$

So far, the stress distribution in the three regions can be completely determined. The solution of Eq. (20), under the conditions (21) and (22) can be written as for the three regions

$$\bar{\sigma}^{\mathrm{f}}_{zj} = A_{j1} + \mathrm{e}^{-\sqrt{g_{j1}}\bar{z}}A_{j2} + \mathrm{e}^{\sqrt{g_{j2}}\bar{z}}A_{j3} \tag{23}$$

where A_{ij} are given in Appendix.

2.5. Numerical application for a pulled out process

We take TiNi SMA fibers and a polymeric matrix (epoxy material) as an example, the material constants are: $E^{\mathrm{m}} = 2.0$ GPa, $v_m = 0.4$, $\alpha^{\mathrm{m}} = 75\times10^{-6}$/°C; $E^{\mathrm{f}} = 30$ GPa, $v^{\mathrm{f}} = 0.3$, $\alpha^{\mathrm{f}} = 6.6\times10^{-6}$/°C, $T_0 = 20$ °C, $M^{\mathrm{os}} = 23$ °C, $M^{\mathrm{of}} = 5$ °C, $C^{\mathrm{M}} = 11.3$ MPa/°C, $\Omega = -0.91\times10^{3}$ MPa. When $T = 30$ °C, $\bar{a}^{\mathrm{M}} = -0.0758$/°C, $\bar{b}^{\mathrm{M}} = -5206$/MPa and $T = 40$°C, $\bar{a}^{\mathrm{M}} = -0.0584$/°C, $\bar{b}^{\mathrm{M}} = -3278$/MPa. The other material constants will be specified when used.

2.5.1. Stress distribution without thermal effect

Let $\delta T = 0$, Fig. 3 shows the distribution of the normalized axial stress as function z/L for different volume fractions of SMA fibers, the applied stress is $\sigma_{\mathrm{a}}/E^{\mathrm{f}} = 0.02$, the embedded length $L = 100$ μm. The results with an elastic fiber (it has the same material constants without transformation) are also included for comparison. It is seen that the transformation relaxes significantly the axial stress in the SMA fiber compared to the elastic case, the volume fraction of fibers also influences the stress distribution, the larger the volume fraction, the larger the axial stress for both SMA fibers and elastic fibers. The influence of the embedded length on the stress distribution is also illustrated in Fig. 4, which shows that embedded length has also important influence on the axial stress distribution.

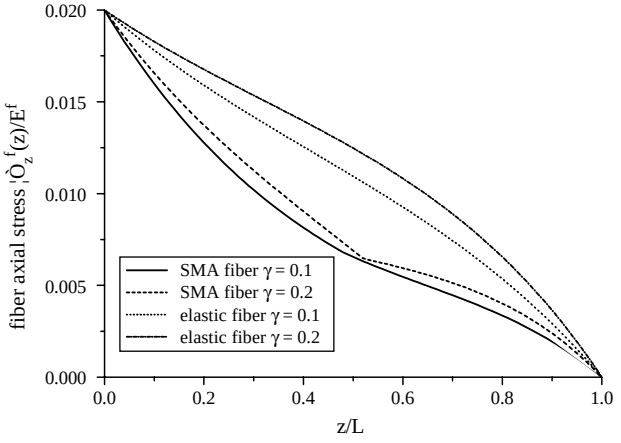

Fig. 3. Influence of fiber volume fraction and transformation on fiber axial stress distribution.

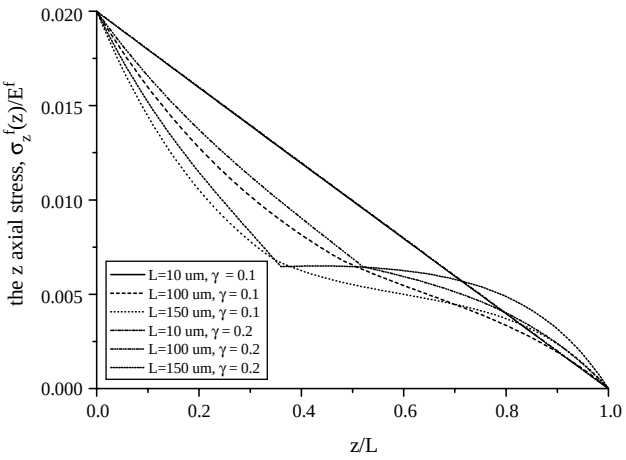

Fig. 4. Influence of embedded length and volume fraction on axial stress distribution in a SMA fiber.

The radial stress distribution along the SMA fiber and the corresponding elastic fiber at different volume concentrations are presented in Fig. 5, it is clearly shown that the large contraction due to the transformation increases significantly the radial stress in the transformed region. This enhanced radial stress in the SMA fiber converges to the result for the elastic fiber in the no transformation region, as expected. This large radial stress is detrimental and tends to open the interface between the SMA fiber and the matrix, a propagation of a ring crack can then take place.

Fig. 6 gives the volume fraction of the martensite in the SMA fiber as function of axial position along the SMA fiber, it can be seen that with an increase of volume fraction of SMA fibers, the complete transformation zone increases, there are large partial transformation zones for these two considered volume concentrations.

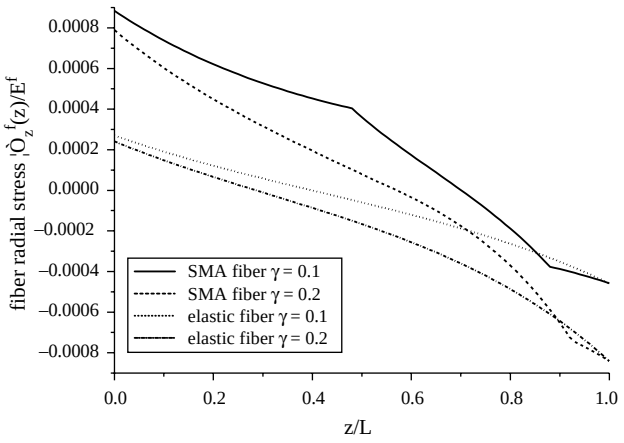

Fig. 5. Influence of fiber volume fraction and transformation on fiber radial stress distribution.

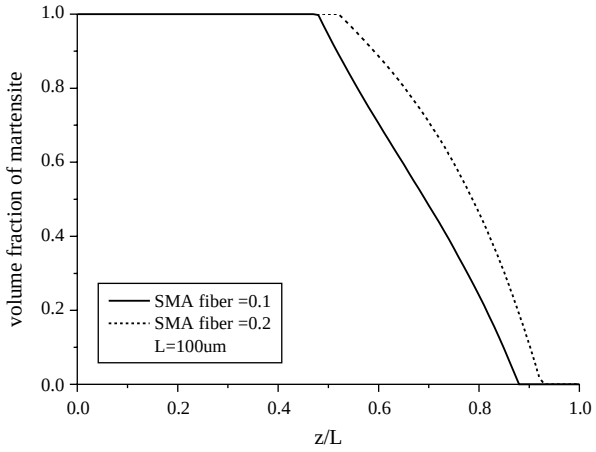

Fig. 6. Variation of martensite volume fraction along SMA fiber.

2.5.2. Stress distribution with thermal effect

Two temperature variations are considered $T=30$ and 40 °C, corresponding to the temperature variations $\delta T=10$ and 20 °C, respectively. The applied stress is still kept as $\sigma_a/E^f=0.02$, and $\gamma=10\%$. Fig. 7 illustrates the axial stress distributions in the SMA fiber for the two considered temperature variations, the comparison with the corresponding elastic fibers with thermal effect is also included. These small variations of temperature have little influence on the axial stress distribution for the elastic fiber, however, they may have significant impact for the SMA fiber. An increase of temperature delays the martensite transformation, as shown in Fig. 9, compared to the case of no thermal effect. The radial stress distribution in the SMA fiber is given in Fig. 8, as indicated in Section 2.4, the transformation of the martensite phase leads to a large lateral contraction, and this increases significantly the radial stress in the transformed region.

Fig. 9 shows the volume fraction of martensite along the SMA fiber for the two considered temperature variations. It is seen that an increase of temperature delays the transformation. For a constant applied stress, an increase of temperature

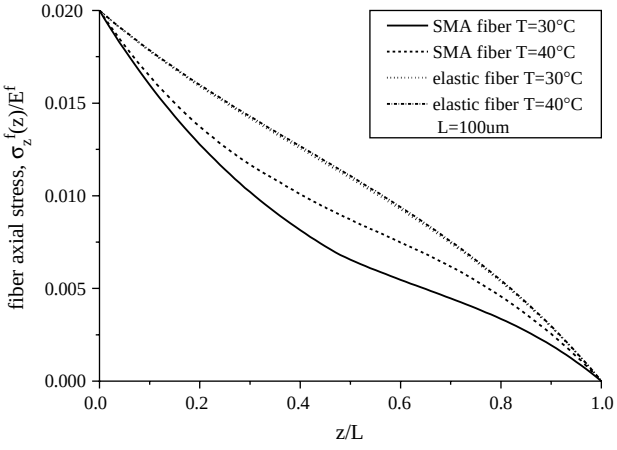

Fig. 7. Effect of temperature on fiber axial stress distribution.

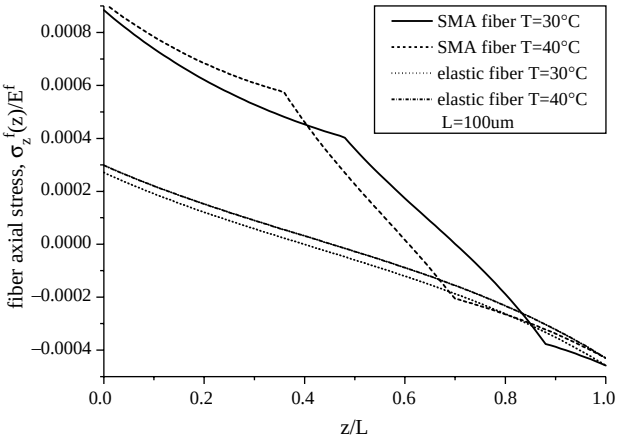

Fig. 8. Influence of temperature on fiber radial stress distribution.

enhances the in situ martensite start and finish temperature, and makes the SMA material difficult to transform.

3. Bridging analysis

3.1. Stress intensity formulation for SMA fiber reinforced composites

We consider a two-dimensional plate having a central crack of a length $2d$ bridged by SMA fibers (with a bridging stress σ_a), the plate is loaded by remote stress σ_b, which is shown in Fig. 10. From Ref. [23], the stress intensity at the tip of the crack K_{Itip} can be evaluated by integrating the stress $\sigma(x)$, acting along the crack (here assuming that the crack is all bridged), multiplied with a weight function $m(x,d)$:

$$K_{Itip}=\int_0^d m(x,d)\times\sigma(x)\mathrm{d}x \tag{24}$$

where d is the half crack length, x represents the position on the crack surface, $\sigma(x)$ consists of the remote applied stress

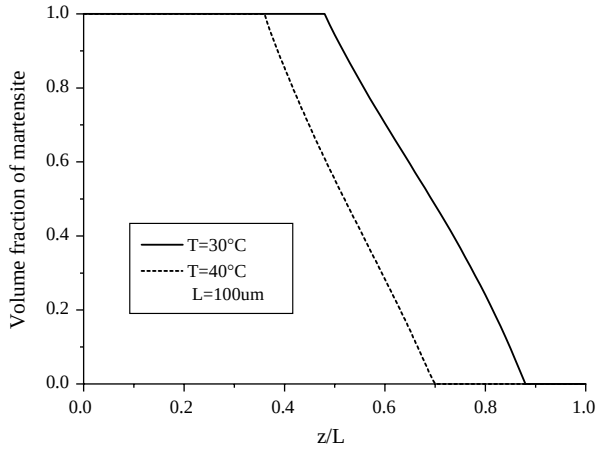

Fig. 9. Distribution of martensite volume fraction in the SMA fiber for different temperatures.

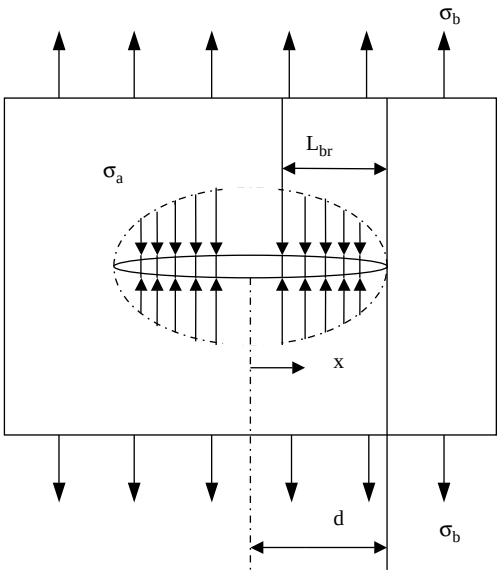

Fig. 10. Schematic figure of a straight crack in a composite plate.

$\sigma_b(x)$ and the bridging stress $\sigma_a(x)$ produced by the SMA fibers. Eq. (24) now becomes:

$$K_{Itip} = \int_0^d m(x,d) \times (\sigma_b(x) - \sigma_a(x))\mathrm{d}x \tag{25}$$

For a straight central crack in an infinite plate, and the expression of $m(x,d)$ is relatively simple, and it is given by [24]:

$$m(x,d) = \sqrt{\frac{d}{\pi(d^2 - x^2)}} \tag{26}$$

From Eq. (25), we see that the estimation of the bridging stress $\sigma_a(x)$ during loading is the key point to determine the stress intensity factor.

3.2. Evaluation of bridging stress

In Section 2, we have proposed a model to analyze the pull-out process for a SMA fiber from an elastic matrix. Relations between the applied load on the SMA fiber and fiber displacement have been derived, which are shown in Figs. 11 and 12, the force–displacement for the corresponding elastic fibers is also included for comparison. It is found that due to the transformation, the force–displacement curve becomes nonlinear for the SMA fiber, the force–displacement curves contained two clear transitions with significant change in slope, the first transition corresponds to the initiation of transformation in the SMA fiber, and the second transition is believed to correspond to the formation of a totally transformed region, these two transitions are also observed in the experiment [7]. We also compared our prediction with the experiment performed by Jonnalagadda et al. [7], the following material parameters given by Ref. [7] are used in the modeling. When $T = 30$ °C, we found $\bar{a}^M = -0.0758/°C$, $\bar{b}^M = -5206/\mathrm{MPa}$ and $a = 75$ μm, $b = 950$ μm. $L_e = 1270$ μm, $L = 40000$ μm. The pulled-out force and displacement relation was showed in Fig. 13, a good agreement is observed. It is also found that the influence of temperature on the force–displacement curve is also significant.

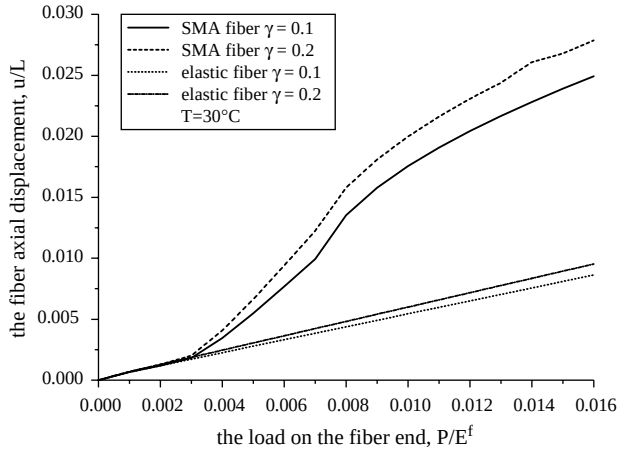

Fig. 11. Force–displacement for a SMA fiber pulled out from an elastic matrix.

Imagine a central crack in a composite plate reinforced by SMA fibers, the SMA fiber will impose a stress F on the surface of the crack. In a continuum approximation, this procedure is equivalent to apply a distributed pressure $\sigma_a(x)$ to the crack surfaces

$$\sigma_a(x) = F\gamma \tag{27}$$

where γ is the volume ratio between SMA fibers and matrix as defined previously.

To simplify the subsequent analysis, in the following, we approximate the force–displacement curves derived from the pull-out analysis by a linear relation with a fitting constant A, which depends on the temperature:

$$u = AF \tag{28}$$

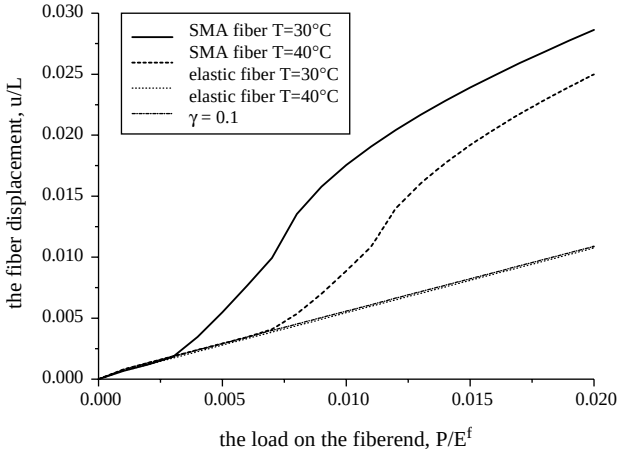

Fig. 12. Force–displacement for a SMA fiber pulled out from an elastic matrix at different temperatures.

From Eqs. (27) and (28), we have

$$u = \frac{A}{\gamma}\sigma_a(x) \tag{29}$$

From Eqs. (25) and (26), it has

$$K_{Itip} = 2\left(\frac{d}{\pi}\right)^{1/2}\int_0^1 \frac{\sigma_b(X)-\sigma_a(X)}{\sqrt{1-X^2}}\,dX \tag{30}$$

where $X = x/d$.

The weight function $m(x,b)$ is a geometry-dependent function and it can be determined by [21]

$$m(x,d) = \frac{E_c'}{K_{Itip}}\frac{\partial u(x,d)}{\partial d} \tag{31}$$

where $E_c' = E_c/(1-\nu_c^2)$ for the plane strain condition, and E_c, ν_c are the elastic modulus and Poisson's ratio of the composite, respectively. From Eqs. (30) and (31), the crack opening at a given position is determined by the distribution of the surface tractions [25]:

$$u(X) = \frac{4(1-\nu_c)d}{\pi E_c}\int_X^1 \frac{s}{\sqrt{s^2-X^2}} \times \int_0^s \frac{[\sigma_b(t)-\sigma_a(t)]dt}{\sqrt{s^2-t^2}}\,ds \tag{32}$$

With help of Eq. (29), the following equation can be derived:

$$\frac{A}{\gamma}\sigma_a(X) = \frac{4(1-\nu_c^2)d}{\pi E_c}\int_X^1 \frac{s}{\sqrt{s^2-X^2}} \times \int_0^s \frac{[\sigma_b(t)-\sigma_a(t)]dt}{\sqrt{s^2-t^2}}\,ds \tag{33}$$

Therefore, Eq. (33) provides a condition to determine the bridging stress distribution along the crack surface. There are various approximate methods to solve Eq. (33) [25–28]. In this paper, we develop the bridging stress $\sigma_a(X)$ into Taylor series, the computed bridging stresses $\sigma_a(X)$ are illustrated in Figs. 13 and 14 for different conditions. In the calculation, we assume the half length of the crack is 3 mm, the material constants are the same as in Section 2. The composite Young's modulus and Poisson ratio

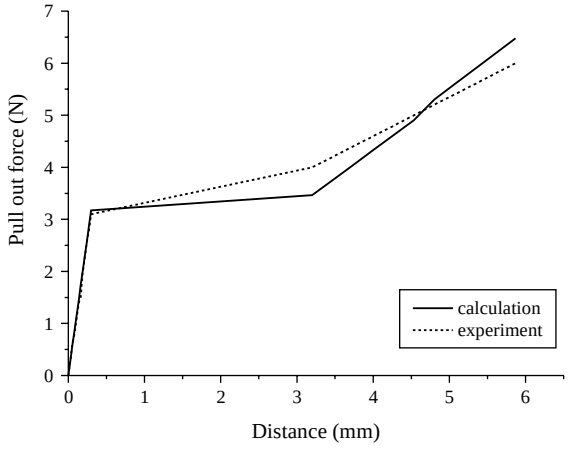

Fig. 13. Pull out force and distance curve: modeling and experiment.

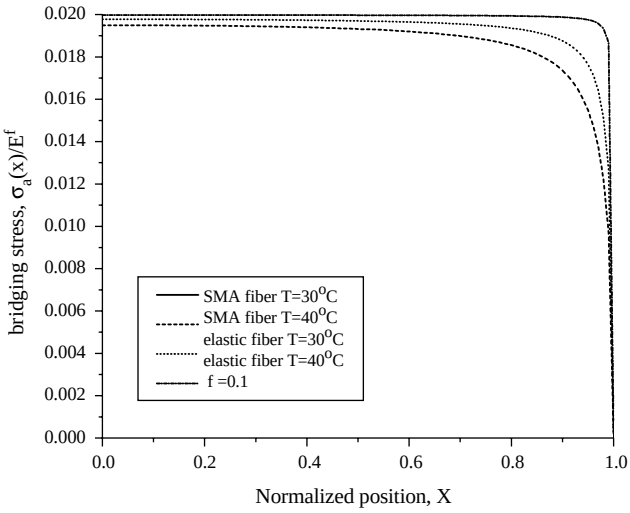

Fig. 14. Bridging stress distribution along crack surface for different fiber volume fractions.

were calculated the mixture law: $E_c = E_f f + E_m(1-f)$, $\nu_c = \nu_f f + \nu_m(1-f)$, where f is volume fraction of the SMA fiber and it is related to γ by $f = \gamma/(1+\gamma)$. The applied load is kept to be $\sigma_b/E^f = 0.02$.

3.3. Influence of temperature variation on stress intensity factor

It can be expected that an increase of temperature delays the martensite transformation, so the bridging effect is more pronounced. Here we impose the macroscopic stress $\sigma_b/E^f = 0.02$, and examine the difference of the stress intensity factor from the actual temperature to a reference temperature. The computed results are shown in Fig. 15 for two fiber concentrations, indeed our calculated results show that an increase of temperature reduces the stress intensity factor, which is in agreement with the experimental observation conducted by Eisaku [6] (Fig. 16).

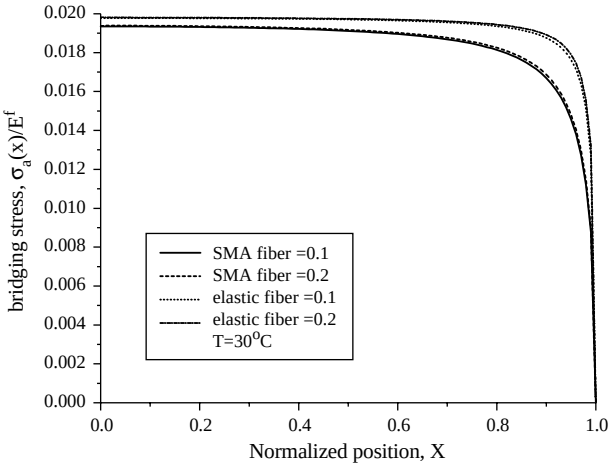

Fig. 15. Bridging stress distribution along the crack surface at different temperatures.

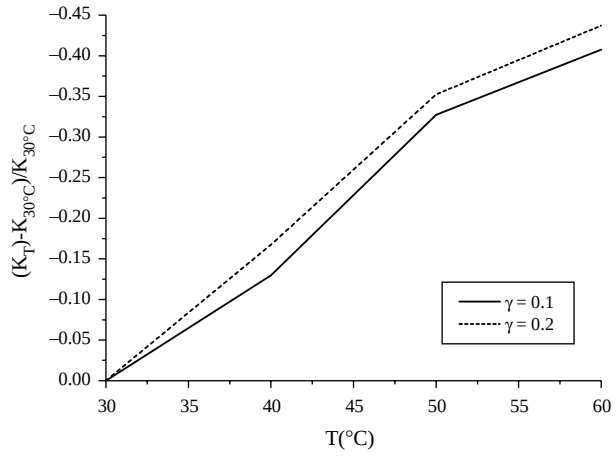

Fig. 16. Variation of stress intensity factor as function of temperature.

4. Conclusions

An analytical model is proposed to analyze the stress transfer during a pull out of a SMA fiber from an elastic matrix. Under an applied stress, the SMA fiber is divided into a fully transformed, a partially transformed and untransformed regions. The stress distributions in each region are determined by a shear-lag method. Numerical calculations show that compared to elastic fiber, the transformation in SMA fiber lowers largely the axial stress, however, the radial stress is increased significantly due to the lateral contraction induced by the transformation. The obtained results are then used to examine the bridging effect due to SMA fibers. The bridging analysis shows that an increase of temperature reduces the stress intensity factor, which is in agreement with experimental observation in literature.

Acknowledgements

The work is supported by national nature science foundation of china through grand 10325210. The authors are grateful to Dr Qingping Sun for his critical reading of the manuscript and the suggestion.

Appendix

(a) Coefficients in Eq. (20)

$$g_{11} = (1 + \alpha\gamma - 2G_1\nu^{\mathrm{f}} - 2\alpha\gamma G_1\nu^{\mathrm{m}})/c$$

$$g_{12} = (-D_{t1z} + 2D_1\nu^{\mathrm{f}} + 2\alpha\gamma D_1\nu^{\mathrm{m}} - \delta T\alpha^{\mathrm{f}} + \delta T\alpha^{\mathrm{m}} + \alpha\gamma\bar{\sigma}_{\mathrm{a}})/c$$

$$g_{21} = (1 + \alpha\gamma - 2G_2\nu^{\mathrm{f}} - 2\alpha\gamma G_2\nu^{\mathrm{m}} + (1 - G_2)D_{t22z}E^{\mathrm{f}})/c$$

$$g_{22} = (-D_{t21z} + 2D_2\nu^{\mathrm{f}} + 2\alpha\gamma D_2\nu^{\mathrm{m}} - \delta T\alpha^{\mathrm{f}} + \delta T\alpha^{\mathrm{m}} + \alpha\gamma\bar{\sigma}_{\mathrm{a}} + D_2D_{t22z}E^{\mathrm{f}})/c$$

$$g_{31} = (1 + \alpha\gamma - 2G_3\nu^{\mathrm{f}} - 2G_3\alpha\gamma\nu^{\mathrm{m}})/c$$

$$g_{32} = (2D_3\nu^{\mathrm{f}} + 2\alpha\gamma D_3\nu^{\mathrm{m}} - \delta T\alpha^{\mathrm{f}} + \delta T\alpha^{\mathrm{m}} + \alpha\gamma\bar{\sigma}_{\mathrm{a}})/c$$

and

$$c = \frac{1}{4}\frac{\alpha(1+\nu^{\mathrm{m}})}{(1+\nu^{\mathrm{f}})}\left[(1+\gamma)^2\ln\left(\frac{1+\gamma}{\gamma}\right) - \left(\frac{3}{2}+\gamma\right)\right]$$

(b) The coefficients A_{ij}

$$A_{j1} = \frac{g_{j2}}{g_{j1}}$$

$$A_{12} = \frac{\mathrm{e}^{\sqrt{g_{11}}l_1}\left(g_{12} - \mathrm{e}^{\sqrt{g_{11}}l_1}g_{12} + \mathrm{e}^{\sqrt{g_{11}}l_1}g_{11}\bar{\sigma}_{\mathrm{a}} - g_{11}\sigma_z^{\mathrm{f}}(\xi=1)\right)}{-1 + \mathrm{e}^{2\sqrt{g_{11}}l_1}}$$

$$A_{13} = \frac{\left(g_{12} - \mathrm{e}^{\sqrt{g_{11}}l_1}g_{12} - g_{11}\bar{\sigma}_{\mathrm{a}} - \mathrm{e}^{\sqrt{g}l_1}g_{11}\sigma_z^{\mathrm{f}}(\xi=1)\right)}{-1 + \mathrm{e}^{2\sqrt{g_{11}}l_1}}$$

$$A_{22} = \frac{\mathrm{e}^{\sqrt{g_{21}}(l_1+l_2)}\left(g_{22} - \mathrm{e}^{\sqrt{g_{21}}l_2}g_{22} + \mathrm{e}^{\sqrt{g_{21}}l_2}g_{21}\sigma_z^{\mathrm{f}}(\xi=1) - g_{21}\sigma_z^{\mathrm{f}}(\xi=0)\right)}{-1 + \mathrm{e}^{2\sqrt{g_{21}}l_2}}$$

$$A_{23} = \frac{\mathrm{e}^{-\sqrt{g_{21}}l_1}\left(g_{22} - \mathrm{e}^{\sqrt{g_{21}}l_2}g_{22} - g_{21}\sigma_z^{\mathrm{f}}(\xi=1) + \mathrm{e}^{\sqrt{g_{21}}l_2}g_{21}\sigma_z^{\mathrm{f}}(\xi=0)\right)}{-1 + \mathrm{e}^{2\sqrt{g_{21}}l_2}}$$

$$A_{32} = \frac{\mathrm{e}^{\sqrt{g_{31}}(l_1+l_2+l)}\left(\left(\mathrm{e}^{\sqrt{g_{31}}l} - \mathrm{e}^{\sqrt{g_{31}}(l_1+l_2)}\right)g_{32} - \mathrm{e}^{\sqrt{g_{31}}l}g_{31}\sigma_z^{\mathrm{f}}(\xi=0)\right)}{-\mathrm{e}^{2\sqrt{g_{31}}l} + \mathrm{e}^{2\sqrt{g_{31}}(l_1+l_2)}},$$

$$A_{33} = \frac{\left(\mathrm{e}^{\sqrt{g_{31}}l} - \mathrm{e}^{\sqrt{g_{31}}(l_1+l_2)}\right)g_{32} + \mathrm{e}^{\sqrt{g_{31}}(l_1+l_2)}g_{31}\sigma_z^{\mathrm{f}}(\xi=0)}{-\mathrm{e}^{2\sqrt{g_{31}}l} + \mathrm{e}^{2\sqrt{g_{31}}(l_1+l_2)}}$$

where $\bar{\sigma}_z^{\mathrm{f}}(\xi = 1)$, $\bar{\sigma}_z^{\mathrm{f}}(\xi = 0)$ are the normalized axial stresses of the SMA fiber where the martensite volume fraction equals to 1 and 0, respectively, they are determined by Eq. (22a) and (22b).

References

[1] Hu GK, Sun QP. Thermal expansion of composites with shape memory alloy inclusions and elastic matrix. Composite Part A 2002; 33:717–24.

[2] Masuda A, Noori M. Optimization of hysteretic characteristics of damping devices based on pseudoelastic shape memory alloys. Int J Non-Linear Mech 2002;37(8):1375–86.

[3] Duval L, Noori MN, Hou Z, Davoodi H, Seelecke S. Random vibration studies of an SDOF system with shape memory restoring force. Physica B 2000;275:138–41.

[4] Birman V. Review of mechanics of shape memory alloy structures. Appl Mech Rev 1997;50:629–45.

[5] Song GQ, Sun QP, Cherkaoui M. Role of microstructures in the thermomechanical behavior of SMA composites. J Eng Mater Technol 1999;121:86–92.

[6] Eisaku U. Improvement in separation of SMA from matrix in SMA embedded smart structures. Mater Sci Eng 2000;A285:363–9.

[7] Jonnalagadda K, Kline GE, Scottos NR. Local displacement and local load transfer in shape memory alloy composites. Exp Mech 1997;37: 78–85.

[8] Jonnalagadda K, Scottos NR, Qidwai MA, Lagoudas DC. In situ displacement measurements and numerical predictions of embedded SMA transformation. Smart Mater Struct 2000;9:701–10.

[9] Cox HL. The elasticity and strength of paper and other fibrous materials. Br J Appl Phys 1952;3:72–9.

[10] Gao YC. Fracture of fiber-reinforced materials. J Appl Math Phys (ZAMP) 1988;39:551–72.

[11] Nairn JA. On the use of shear-lag methods for analysis of stress transfer in unidirectional composites. Mech Mater 1997;26:63–80.

[12] Hutchinson JW, Jensen HM. Model of fiber debonding and pullout in brittle composites with friction. Mech Mater 1990;9:139–63.

[13] Hsueh CH. Pull-out of a ductile fiber from a brittle matrix, Part1: Shear Lag Model. J Mater Sci 1994;29:4793–801.

[14] Fu SY, Yue CY, Hu X, Mai YW. Analysis of the micromechanics of stress transfer in single- and multi-fiber pull-out tests. Compos Sci Technol 2000;60:569–79.

[15] Hsueh CH. Interfacial debonding and fiber pull-out stresses of fiber-reinforced composites, VII: Improved analyses for bonded interface. Mater Sci Eng 1992;154:125–32.

[16] Lu GY, Mai YW. Effect of plastic coating on fiber–matrix interface denbonding. J Mater Sci 1995;30:5872–8.

[17] Aleksandrov SY, Gol'dshtein RV. Pull-out of a rigid fiber from an elastoplastic matrix. J Appl Math Mech 2000;64:155–61.

[18] Lagoudas DC, Boyd JG, Bo Z. Micromechanics of active composites with SMA fibers. J Eng Mater Technol 1994;116:337–47.

[19] Lu ZK, Weng GJ. Martensitic transformation and stress–strain relations of shape-memory alloys. J Mech Phys Solids 1997;45: 1905–28.

[20] Sun QP, Hwang KC. Micromechanics modeling for the constitutive behavior of polycrystalline shape memory alloys: I. Derivation of general relations; II. Study of the individual phenomena. J Mech Phys Solids 1993;41:1–33.

[21] Huang MS, Brinson LC. Multivariant model for single crystal SMA behavior. J Mech Phys Solids 1998;46:1379–409.

[22] Xu ZL. Elasticity theory. Gao Deng Jiao Yu Chu Ban She, Beijing 1990;170 [in Chinese].

[23] Raddatz O, Schenider GA, Claussen N. Modelling of R-curve behaviour in ceramic/metal composites. Acta Mater 1998;46: 6381–95.

[24] Cox BN, Marshall DB. Stable and unstable solutions for bridged cracks in various specimens. Acta Metall. 1991;39:341–63.

[25] Marshall DB, Cox BN. The mechanics of matrix cracking in brittle-matrix fiber composites. Acta Metall 1985;33:2013–21.

[26] Budiansky B, Amazigo JC. Toughening by aligned, frictionally constrained fibers. J Mech Phys Solids 1989;37:93–109.

[27] Budiansky B, Hutchinson JW, Evans AG. Matrix fracture in fiber-reinforced ceramics. J Mech Phys Solids 1986;34:167–89.

[28] Liu YF, Masuda C, Yuuki RJ. Effect of microstructural parameters on the fracture behavior of fiber-reinforced ceramics. Mech Mater 1998; 29:111–21.